Journal of Non-Crystalline Solids 568 (2021) 120964

Contents lists available at ScienceDirect

Journal of Non-Crystalline Solids

journal homepage: www.elsevier.com/locate/jnoncrysol

Vanadyl doped Li-zinc borate glasses: Optical and ESR study

M. Farouk [a,*], H.M. Mokhtar [b], Z.M. Abd El-Fattah [a], A. Samir [c]

[a] Physics Department, Faculty of Science, Al-Azhar University, Nasr City, Cairo, 11884, Egypt
[b] Physics Department, Faculty of Science, Al-Azhar University (Girls Branch), Nasr City, Cairo, Egypt
[c] Engineering Mathematics and Physics Department, Faculty of Engineering at Shoubra, Benha University, Cairo, 11629, Egypt

ARTICLE INFO

Keywords:
Vanadium borate glass
FTIR spectra
ESR spectra
Optical absorption spectra

ABSTRACT

Glasses with the composition xV_2O_5-(15-x) Li_2O-70B_2O_3-15ZnO, for x varies from 0 to 4 mol. %, were synthesized using standard quenching technique. The amorphous nature for selected samples (x= 0, 1 and 4 mol. %) was ensured from X-ray diffraction (XRD) measurements. The samples were found to compose mainly from BO_3 and BO_4 basic structural units as inferred from Fourier transform infrared (FTIR) data. The number of BO_4 (BO_3) structural units was found to decrease (increase) with increasing the number of NBOs. These structural modifications within the glass network are responsible for the here observed composition dependence optical energy gap (E_{otp}) and Urbach band tail (ΔE). The electron spin resonance (ESR) results revealed a tetragonal compression for VO^{2+} ions present in octahedral coordination, with distinct optical transitions in the visible spectral regime.

1. Introduction

Borate glasses doped with Transition metal (TM) ions are gaining much attention due to their distinguished optical, electrical, and luminescent properties suitable for multiple potential applications [1–6]. They possess several attractive features including costless and ease of preparation as well as high chemical durability [7]. Vanadium oxide (V_2O_5), in particular, with its pyramidal VO_5 structural units within glass networks, offers high electrical conductivity stemming from mutual electronic hopping between V^{4+} and V^{5+} ions [8–12].

These properties make borate glasses containing V_2O_5 oxides highly suitable for many applications, such as memory and switching devices. In additions, the presence of lithium oxide in high quantities within glass networks renders these glasses as efficient ionic conductors and can, therefore, be integrated in solid-state batteries as promising electrolyte materials [13–15].

Within glasses network, V_2O_5 can act as a conditional glass former depending on the initial glass constituents [16]. Likewise, zinc oxide (ZnO) in borate glasses can simultaneously act as glass former and modifier. Glass modifiers generally introduce coordinated defects and NBO atoms as they break up the B-O-B bonds. In the case of ZnO modifier, this leads to octahedral coordination for Zn^{2+} ions [16,17]. Alternatively, when Zn is tetrahedrally bonded to oxygen ions, the glass network is composed from pyramidal ZnO_4 structural units linked to BO_4 units through B-O-Zn bonds all over the entire glass network [18]. These zinc-contained borate glasses are often characterized by high thermal stability and insulating strength as well as good optical transparency over a wide wavelength range [19–21]. Electron spin resonance (ESR) spectroscopy of TM ions in amorphous materials is an interesting and ongoing research subject as it provides a simple route to explore the materials structure. It gives valuable knowledge about the TM ions valence state and local environment (*i.e.*, the ligand field). TM ions are distinguished by their outer *d* electrons orbital with uniquely broad radial distributions and high sensitivity to crystal fields and are, therefore, considered as efficient glass structure probe [22]. In this context, Vanadyl ion is often used as an efficient probe for glasses structure, because of its highly featured ESR spectra that exhibits well resolved hyperfine structure (rhs) at room temperature, arising from unpaired electrons ($3d^1$) with ^{51}V isotope (nuclear spin 7/2). Although vanadium offers two oxidation states, namely diamagnetic and paramagnetic V^{5+} and V^{4+}, respectively, the ESR spectra exclusively originates from V^{4+} ions [23]. Nonetheless, it is also possible that V^{5+} are partially converted into V^{4+} ions during the melting process. While V^{5+} ions participate structural units in network forming positions in the form of trigonal bipyramidal VO_5, the modifiers V^{4+} ions form VO^{2+} complexes that distort the glass network [24].

In order to combined the high thermal stability and optical transparency offered by ZnO, with the multivalency and optical and

* Corresponding author.
E-mail address: m_farouk@azhar.edu.eg (M. Farouk).

https://doi.org/10.1016/j.jnoncrysol.2021.120964
Received 12 March 2021; Received in revised form 4 May 2021; Accepted 27 May 2021
Available online 10 June 2021

hyperfine characteristics of V_2O_5, the composition xV_2O_5-(15-x) Li_2O-$70B_2O_3$-15ZnO has been selected as the glass system. The presence of co-doped zinc and vanadium ions in the lithium borate glasses may find potential applications in optical devices and optoelectronic devices.

The present work subjected to study the modification introduced to the borate network by the addition of a fixed amount of ZnO and variable concentrations of vanadium oxide. The structural changes, particularly those affecting the borate structural units, were inferred from density, molar volume, and FTIR investigations, while the optical properties and oxidation states were obtained from optical spectroscopy and ESR studies.

2. Experimental details

Glass samples of molar composition xV_2O_5-(15-x) Li_2O-$70B_2O_3$-15ZnO], where x = 0, 0.5, 1, 2 and 4 mol. %, were synthesized by melt quenching technique. The samples were synthesized from reagent grade H_3BO_3, V_2O_5, ZnO and Li_2CO_3. The chemical powders with the desired composition were all melted in a porcelain crucible heated to 900–1000°C for one hour, using an electric furnace. The molten was quenched between two brass plates to form discs of reduced thickness ~0.2 cm. The undoped glasses have been found to be colorless, while samples containing V_2O_5 exhibit light yellow color, gradually getting darker with increasingV_2O_5 content from 0.5 to 4 mol. %. X-ray diffraction (XRD) data were collected by a Shimadzu XD3A diffractometer. The FTIR spectra of the samples were recorded in the range (2000–400 cm-1) by a Perkin Elmer IR spectrophotometer, using KBr pellets. The optical absorption spectra of the glass samples were recorded in the 190-1100 nm range using a JASCO V670 spectrophotometer with ±1 nm resolution. The electron spin resonance (ESR) data were collected by X-band frequency (ν= 9.154 GHz) EMX spectrometer (Bruker, Germany). The spectra have been normalized by dividing the ESR signal by the mass of the measured powder. All measurements were carried out at room temperature.

3. Results and discussion

3.1. X-Ray diffraction (XRD)

Fig. 1 presents typical XRD patterns, specifically, for x = 0, 1, and 4 mol.% samples. The absence of discrete sharp peaks over a wide range of diffraction angles justifies the amorphous nature of the samples.

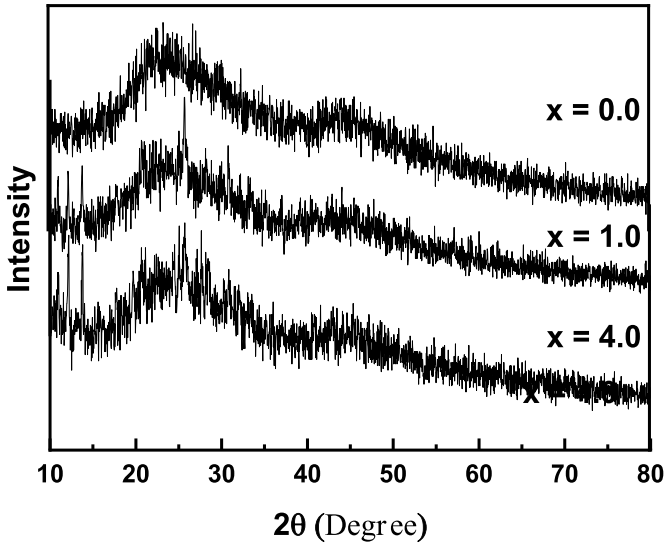

Fig. 1. X-ray diffraction patterns of selected glass samples.

3.2. FT-IR studies

The FTIR absorption spectra for all glass samples are shown in Fig. 2. All spectra feature three broad bands originated from borate structural units. The bands centered at ~ 1400 cm^{-1} and ~1000 cm^{-1} are due BO_3 and BO_4 units, respectively, while the third band at ~700 cm^{-1} belongs to B-O-B linkages of BO_3 units [25]. The broadening of these bands is resulting from the overlap between several individual peaks. Therefore, in order to quantify the presence of individual structural groups within the glass host, a detailed deconvolution of the FTIR spectra is compulsory. Fig. 3 shows such a deconvolution process applied to the spectrum of x = 0.5 mol.% sample, as an example. The deconvolution peaks were assumed to be of Gaussian type. The parameters obtained from such deconvolution process are the individual peak centers (C), as fingerprints of the vibration modes associated with a specific structural group with the corresponding bands assignment listed in Table 1, and the relative area (A), which reflects the concentration of structural units. The bands in the range 1220-1615 cm^{-1} belong to symmetric B-O stretching of the BO3 groups [26,29,30]. The weak small absorption band at 815 cm^{-1} is due to V-O-V chains or V=O stretching mode [31–33]. Absorption bands in the range 881-1103 cm-1 are assigned as B-O stretching modes within BO4 units. The band at ~881 cm^{-1} corresponds to the stretching of non-bridging oxygen's (NBOs) of BO_4 units [26,28].

It is also noticed that the intensity of these bands decreases, and their position shifts towards higher wave numbers with the gradual addition of V_2O_5. This indicates that the number of BO_3 units increase at the expense of BO_4 with increasing number of NBOs. The fraction of BO_4 units (N_4) deduced from the relative areas as $BO_4/(BO_3+BO_4)$ [25–27], was found to decrease with increasing V_2O_5 content, as displayed in Fig. 4. This indicates the conversion of the structural units from BO_4 to BO_3. Consequently, the NBOs would start to form and randomize the glass structure. Therefore, the incorporation of V_2O_5 into the glass network breaks the regularity of the borate rings structure and causes the formation of ortho-borate groups.

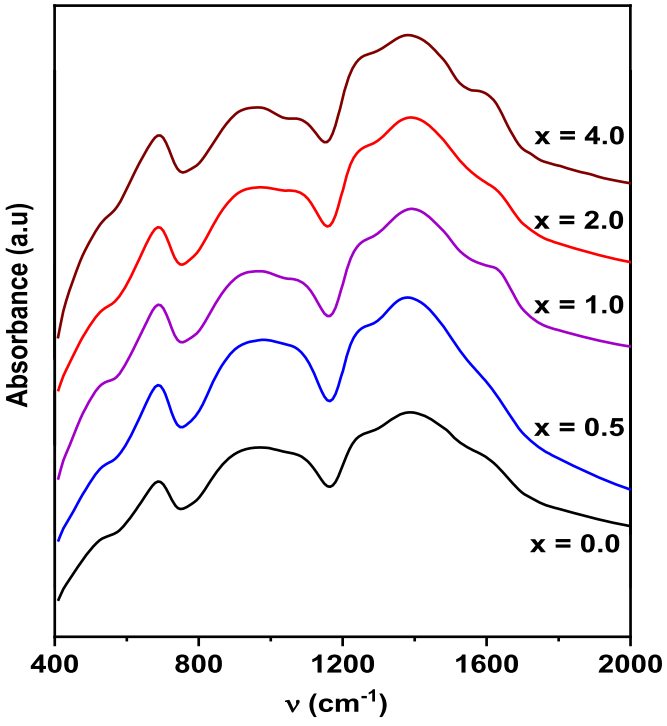

Fig. 2. FTIR spectra for all glass samples of different V_2O_5 concentrations.

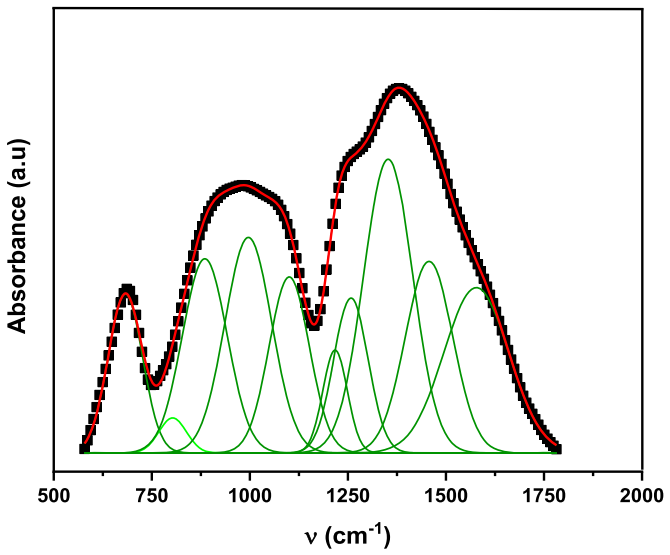

Fig. 3. Example highlighting the deconvolution process applied to the infrared bands for x= 0.5 mol.%.

Table 1
Band assignments of FTIR spectra for $x$$V_2O_5$-(15-$x$) Li_2O-70B_2O_3- 15ZnO glasses.

Band center c (cm^{-1}) / Relative area A					Band assignments
x =0	x =0.5	x =1	x =2	x =4	
685	682	673	685	685	Bending vibrations of B-O-B linkages in borate network
4.1	10.6	3.73	5.8	3.7	
881	885	956	899	1007	Stretching vibrations of the non-bridging oxygen's (NBOs) of BO_4 groups and is merged with V=O stretching mode or V-O-V chains.
10.4	16.84	5.6	15.6	6.2	
996	996	975	1026	1033	B-O stretching in BO_4 units from tri, tetra and pentaborate groups.
15.1	19.5	16.5	14	9.5	
1102	1100	1095	1104	1103	
7.4	13.7	3.1	4.7	2.1	
1220	1217	1240	1228	1222	B-O stretching vibrations of trigonal BO_3 units involving mainly the linkage oxygen connecting different groups.
4.4	4.88	8.1	7.9	3.7	
1274	1257	1356	1328	1361	linkage of boron atom with three oxygen atoms.
10.4	10.31	16.8	26.2	4.5	
1369	1352	1356	1346	1334	
16.2	27.9	10.2	24.2	17.1	
1459	1457	1469	1462	1461	Stretching vibrations of the B-O of trigonal $(BO_3)^{3-}$ units in metaborates, pyroborates.
4.3	4.6	4.5	4.8	4.7	
1542	1577	1606	1615	1615	B-O asymmetric stretching vibrations of BO_3 units.
28.19	28	13	4	10	

3.3. Density and molar volume

In oxide glasses, density measurement is a powerful tool that can easily detect any micro-structural changes in glass network. It is affected by the structural softening or compactness. Generally, the density (ρ) and molar volume (V_M) of a glassy system follow an inverse trend, which is clearly observed in this work [34]. The measured density and estimated molar volume are presented in Table 1, and are plotted in Fig. 5 for all glass samples as a function of vanadium concentration. It is clear that the density decreases, whereas V_M increases, with increasing the concentrations of vanadium content. The overall increase in V_M is likely due to the larger ionic radii of V_2O_5 compared to Li^+ ions, which can result in the formation of excess free volume. As V_2O_5 content increases, there is a shift in boron's coordination (conversion of BO_3 into BO_4 units) due to the availability of more oxygen from V_2O_5. Since the molecular mass of V_2O_5 is higher than Li_2O, an increase in the molar volume is expected. The increase in V_M may also indicate that the number of NBO produced by the addition of V_2O_5 is greater than that produced by an equivalent quantity of Li_2O. The increased V_M of the molecular mass, thus, causes a decrease in its density [35,36], in agreement with FTIR results discussed above.

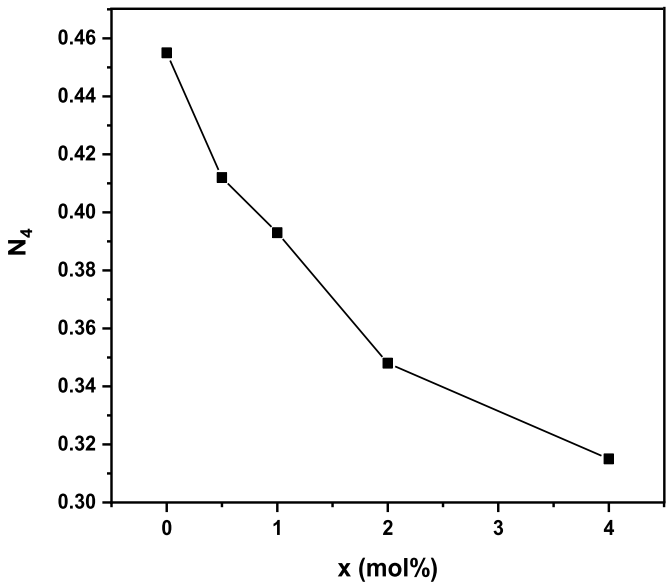

Fig. 4. Variation of N_4 with V_2O_5 content.

3.4. Optical properties

The optical absorption spectra for all glass samples are shown in Fig. 6. The spectra are composed of an absorption edge and a strong UV-Vis absorption band, both gradually shifting towards higher wavelength (*i.e.*, red shift) with increasing V_2O_5 content. For glass samples containing V_2O_5, the UV absorption band is found to be highly broadened

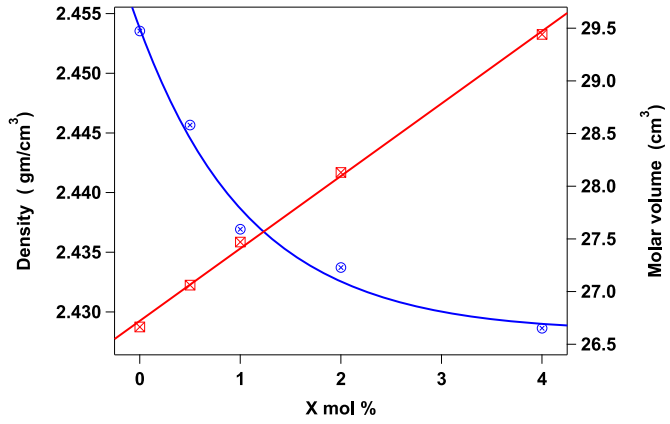

Fig. 5. Density and molar volume for all V_2O_5 doped glass samples.

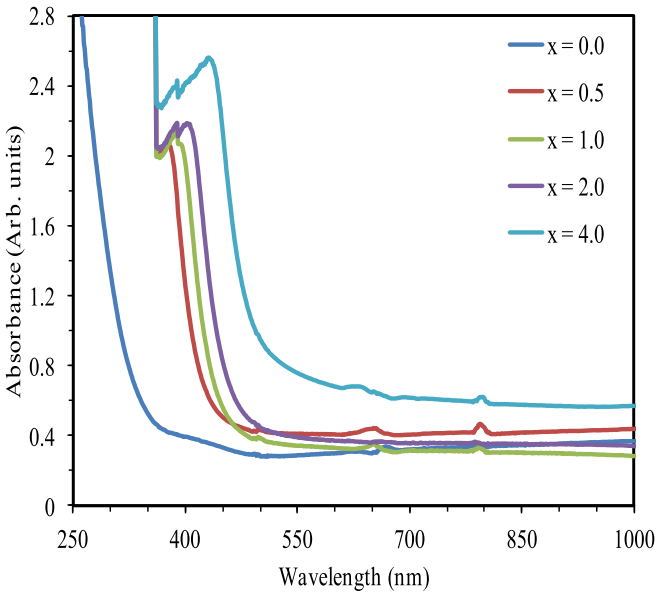

Fig. 6. Optical absorption spectra of all samples.

and extended into the longer wavelength spanning from 361 to 436 nm (*i.e.*, red-shifted) with increasing *x* mol. %. This shift reflects changes in boron coordination (BO_4 to BO_3) and N_4 values, consistent with FTIR results. A careful inspection of optical spectra allows the affirmation that VO^{2+} ions are present in octahedral sites with tetragonal-distortion. This remark is based on the identification of an intense absorption band characteristic for $^2B_{2g} \rightarrow {}^2A_{1g}$ transition of VO^{2+} ions [37–40].

The absorption coefficient (**α**) is the main factor in determining the parameters $(\alpha h\nu)^{0.5}$ and ln(**α**) for high and low absorption, respectively. The size of optical band gap (E_{opt}) is estimated from the following equation [41,42]

$$\alpha h\nu = B\left(h\nu - E_g\right)^n$$

where hν is the incident photon energy and B is a constant. As shown in Fig. 7, the n = 2 value yields the best fit to absorption edge, as expected for most glassy systems with allowed indirect band transition. The optical band gap E_{opt} was found to decrease with increasing vanadium contents, as displayed in Fig. 8. This due to large overlap between the localized electrons from V^{4+} ($3d^1$) and V^{3+}($3d^2$) sites with V^{5+} ($3d^0$) sites, facilitated by the creation of many donor centers at higher V^{4+} and V^{3+} ions concentration [33]. In addition, the increase in the network modifier enhances the NBOs concentration, thereby shifting the valance band minimum to higher energies and reduces the optical band gap [43]. Thus, the addition of V_2O_5 causes the breaking of the regular structure of the rings (borate and boroxol) and the appearance of orthoborate groups [8]. For the sake of completeness, it should be noted that the optical transitions from vanadium are close in energy to the absorption edge and could, therefore, lead to large underestimation of the gap size as reported earlier for TM doped glasses [44–46]. The energy dependence of ln(**α**) parameter facilitates the investigation of the width of the localized states (Urbach energy, ΔE) using the following formula [47]

$$\alpha(\nu) = C \exp^{\frac{h\nu}{\Delta E}}$$

where C is a constant. The values (ΔE) were calculated following the standard recipe, i.e., by acting on the linear portion of ln(α) vs hν curves and constructing the reciprocals of their slopes. The ΔE values are displayed in Fig. 8 for all samples. While the optical band gap undergoes size reduction with V_2O_5 contents, the reduced number of bridging oxygen's and rigidity both increase the number of localized states (i.e., the donor centers) within the glass network and cause a red-shift of the edge [43]. For non-crystalline materials the typical values of ΔE lie within the range 0.045 to 0.66 [48]. In the present samples the ΔE values have been found to lie within and almost at the center of the reported range. The relation between the refractive index (n) and E_{opt} can be estimated using the relation [49]

$$\frac{n^2 - 1}{n^2 + 1} = 1 - \sqrt{\frac{E_g}{20}}$$

The linear refractive index (n) was found to increase gradually with the vanadium ratio as shown Fig. 9, in agreement with earlier literature [43,50].

The nonlinear refractive index, as estimated from its dependence on the static index, was found to linearly increase by a factor of ~2.6 (from 5.96 to 15.44 × 10^{-11} esu) suggesting possible applications for the highest doped samples in nonlinear optics.

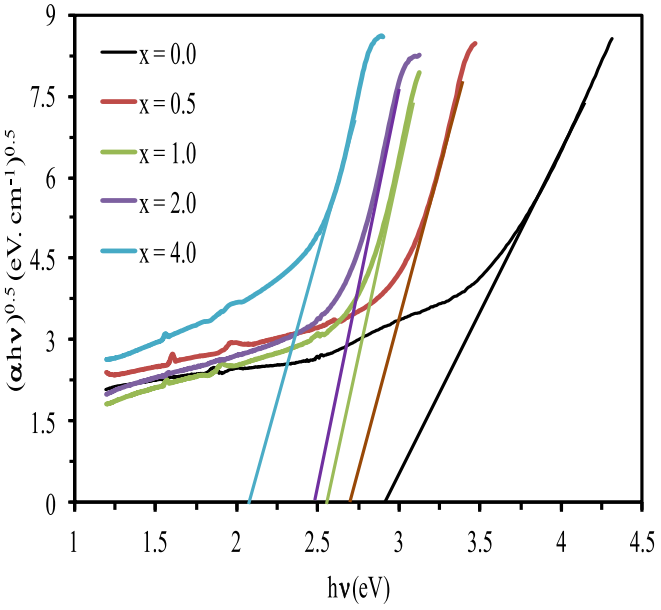

Fig. 7. Tauc's plots of the investigated samples.

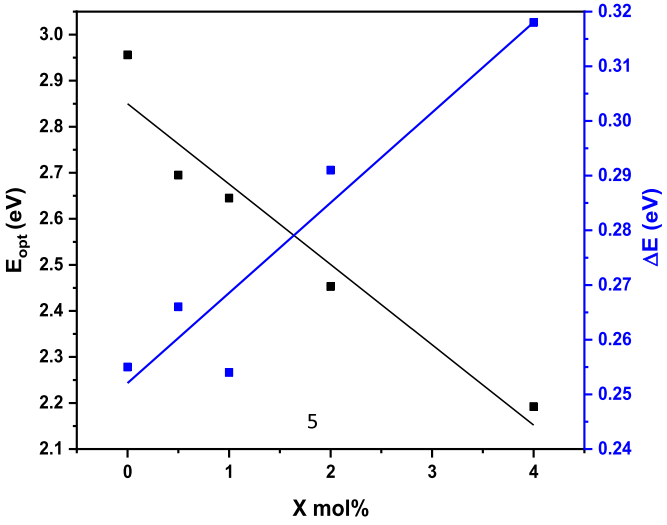

Fig. 8. Dependence of the optical band gap (E_{opt}) and Urbach energy (ΔE) on V_2O_5 content.

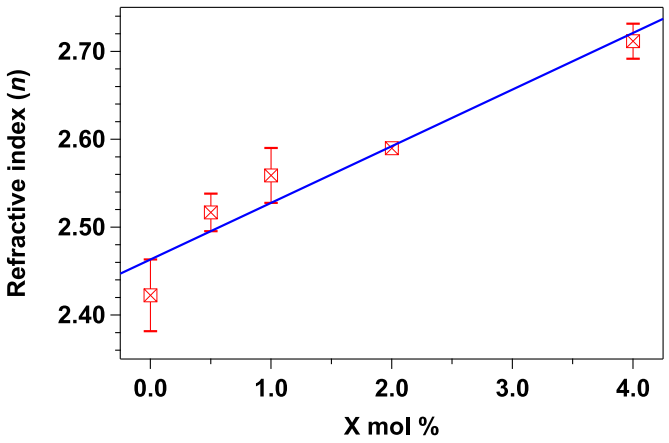

Fig. 9. The variation of the refractive index (n) with V_2O_5 content. The error bars refer to deviations from the linear fitting.

3.5. ESR studies

For the sake of gaining deep insight into vanadium ions incorporated within different systems, the glass samples were investigated by means of ESR. Fig. 10 shows the room temperature ESR spectra for all samples. No ESR signal is observed for the spectrum of the pristine sample (i.e., free-vanadium) reflecting the absence of unpaired electrons. When vanadium contents are gradually added, the intensity and resolving-power of developed vanadium characteristic signals were greatly enhanced. The increased signal intensity indicates an increase of vanadium ions in the tetravalent V^{4+} state within the glass network, which in turn reveals predominant contribution from vanadium ions in tetravalent state with possible V^{5+} traces. This assures the multivalency of V ions and its correlation with the different glass colors here obtained.

The spectra exhibit fine structures composed of eight signals characteristic for the nuclear magnetic quantum numbers: $M_I = \pm 7/2, \pm 5/2, \pm 3/2, \pm 1/2$ following the spin selection rules $\Delta M_I = 0$ and $\Delta Ms = \pm 1$). Such hyperfine interaction is known to originate from unpaired $3d^1$ electron due to dipole-dipole interactions between the magnetic and electronic moments of the nucleus with the electrons of paramagnetic V^{4+} ions [8,23].

The axial spin-Hamiltonians could be used to analyze ESR signals for VO^{2+}ions in glasses. The solutions to such Hamiltonian for the parallel

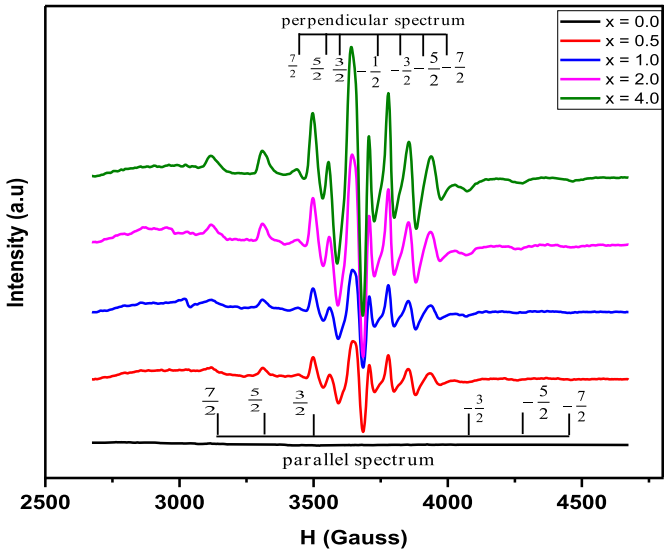

Fig. 10. Room temperature ESR spectra of spin-active V^{2+} ions embedded within the glass system.

and perpendicular hyperfine orientations are given as [23,24,30,51,52]:

$$H_{\parallel}(m_I) = H_{\parallel}(0) - A_{\parallel}(m_I) - \left\{\frac{63}{4} - m_I^2\right\}\left(\frac{A_{\perp}^2}{2H_{\perp}(0)}\right)H_{\perp}(m_I)$$

$$= H_{\perp}(0) - A_{\perp}(m_I) - \left\{\frac{63}{4} - m_I^2\right\}\left(\frac{(A_{\perp}^2 + A_{\parallel}^2)}{4H_{\perp}(0)}\right)$$

The spin-Hamiltonian parameters for VO^{2+} ions present in the glass samples were determined from the following known relation, and are listed in Table 2:

$$H_{\parallel}(0) = \left(\frac{h\nu}{\beta g_{\parallel}}\right) \text{ And } H_{\perp}(0) = \left(\frac{h\nu}{\beta g_{\perp}}\right)$$

Here, ν is the microwave frequency and $H_{||}$ positions for a given m_I were taken at the first derivative maximum of the parallel hfs, while those of $H_{\perp}$ were enclosed between the first derivative perpendicular peak and its zero. The values of $A_{||}$ and $A_{\perp}$, as tabulated in Table 2, follows from the equation:

$$A_{\parallel} = \frac{1}{7}\left(H_{\parallel}\left(-\frac{7}{2}\right) - H_{\parallel}\left(\frac{7}{2}\right)\right)$$

$$A_{\perp} = \frac{1}{7}\left(H_{\perp}\left(-\frac{7}{2}\right) - H_{\perp}\left(\frac{7}{2}\right)\right)$$

The analysis of the spectra yields $A_{||} > A_{\perp}$ and indicates that VO^{2+} ions exist in octahedral site symmetry. Since $g_{||} < g_{\perp} < g_e$ (where g_e = 2.0023 for free electron value) this symmetry exhibits an additional tetragonal compression, [33], which is clearly reflected in the quantity $\Delta g_{||}/\Delta g_{\perp}$. It is observed that $\Delta g_{||}/\Delta g_{\perp}$ increases with increasing vanadium content which, rather likely, indicating larger tetragonal distortions within the glass [8,43].

3.5.1. Spin density (N)

The density N for spins participating in resonance (V^{4+} ion concentrations) can be estimated from the area under the absorption curve relative to the standard-known concentration as the following formula [24,51]:

$$N = \frac{A_x (P_{std})^{1/2} (Scan_x)^2 G_{std} (H_m)_{std} (g_{std})^2 [S(s+1)]_{std}}{A_{std} (P_x)^{1/2} (Scan_{std})^2 G_x (H_m)_x (g_x)^2 [S(s+1)]_x} [Std]$$

The calculated spin density (N) is tabulated in Table 2. Clearly, the density of spins increases as a result of replacing Li_2O by V_2O_5 content, strictly following the same behavior of the resonance intensity, rather likely due to an increased V^{4+} ratio.

3.5.2. Paramagnetic susceptibility (χ)

The paramagnetic susceptibility (χ) as estimated from ESR parameters can be obtained using the equation [23,51]:

$$\chi = \frac{Ng^2\beta^2 J(J+1)}{3K_B(T)}$$

while the g factor is obtained as $g = (g_{||} + 2g_{\perp})/3$. Table 2 reports the increasing of **(χ)** for higher V_2O_5 contents.

4. Conclusions

In the present work, TM-doped glass samples of composition xV_2O_5–(15–x) Li_2O–$70B_2O_3$– 15ZnO, with x gradually varies from 0 to 4 mol. %, were prepared. XRD patterns confirmed the amorphous character of the prepared glasses. FTIR spectroscopy revealed that incorporation of vanadium content into this glass network facilitates the conversion of the BO_4 structural units into BO_3. The optical band gap energy is decreased and both the refractive index (n) and Urbach energy (ΔE) are increased with increasing V_2O_5 content, indicating more disordered glasses. ESR data revealed the coexistence of both V^{4+} and

Table 2
Spin Hamiltonian parameters, the number of spin density (N), and the paramagnetic susceptibility (χ) of the present glass system.

x mol%	$g_{\|\|}$	$g_{\perp}$	$A_{\|\|}$ x10^{-4} (cm^{-1})	$A_{\perp}$ x10^{-4} (cm^{-1})	$\Delta g_{\|\|}$	$\Delta g_{\perp}$	$\Delta_{\|\|}/\Delta g_{\perp}$	N × 10^{21} (ions/cm^3)	$\chi \times 10^{-3}$ (m^3/kg)
0	-	-	-	-	-	-	-	-	-
0.5	1.872	1.883	177.7	70.1	0.1303	0.1193	1.092	3.37	0.585
1	1.874	1.885	176.7	70.4	0.1283	0.1173	1.093	3.93	0.684
2	1.874	1.887	176.5	71.1	0.1283	0.1153	1.113	8.87	1.543
4	1.876	1.891	176.3	72.0	0.1263	0.1113	1.135	12.73	2.224

V^{5+} within the glass samples. Analysis of ESR spectra showed that $g_{\|\|} < g_{\perp} < g_e$ and $A_{\|\|} > A_{\perp}$, indicating a tetragonal compression of the octahedrally coordinated VO^{2+} ions. The increased value of $\Delta g_{\|\|}/\Delta g_{\perp}$ ratio, with vanadium content, reflects higher degree of octahedral symmetry around the vanadyl ions.

CRediT authorship contribution statement

M. Farouk: Conceptualization, Methodology, Investigation, Writing – original draft. **H.M. Mokhtar:** Methodology, Investigation. **Z.M. Abd El-Fattah:** Visualization, Writing – review & editing. **A. Samir:** Conceptualization, Methodology, Investigation, Writing – original draft, Writing – original draft.

Declaration of Competing Interest

No funding was received for this work.

References

[1] K. Swapna, A.S.Rao SkMahamuda, M. Jayasimhadri, T. Sasikala, L. Rama Moorthy, Visible, J. Mol. Struct. 146 (2014) 255.
[2] N.S. Saetova, A.A. Raskovalov, B.D. Antonov, T.A. Denisova, N.A. Zhuravlev, J. Non-Cryst. Solids 545 (2020), 120253.
[3] M.H.A. Mhareb, S. Hashima, S.K. Ghoshal, Y.S.M. Alajerami, M.A. Salehd, M.M. A. Maqableh, N. Tamchek, Optik 126 (2015) 3638.
[4] H. Wena, P.A. Tannerb, B.-M. Cheng, Mater. Res. Bull. 83 (2016) 400.
[5] H.A. ElBatal, A.M. Abdelghany, I.S. Ali, J. Non-Cryst. Solids 358 (2012) 820.
[6] G.P. Singh, S. Kaur, P. Kaur, S. Kumar, D.P. Singh, Phys. B 406 (2011) 1890.
[7] A. Agarwal, I. Pal, S. Sanghi, M.P. Aggarwal, Opt. Mater. 32 (2009) 339.
[8] M. Subhadra, S. Sulochana, P. Kistaiah, Mater. Today 5 (2018) 26417–26423.
[9] S. Afyon, F. Krumeich, C. Mensing, A. Borgschulte, R. Nesper, Sci. Rep. 4 (2014) 7113.
[10] A.A. El-Moneim, J. Non-Cryst. Solids 514 (2019) 69.
[11] M. Farouka, K. Abdallauh, M. Attallah, Z.M. Abd El-Fattah, J. Non-Cryst. Solids 523 (2019), 119607.
[12] O. Cozar, I. Ardelean, V. Simon, G. Ilonca, C. Crocium, C. Cefan, J. Alloys Compd. 326 (2001) 124.
[13] P. Butnoi, N. Chanlek, Y. Poo-arporn, S. Pinitsoontorn, S. Maensiri, P. Kidkhunthod, J. Alloys Comp., 809, 2019, 151811.
[14] L. Bih, M. El Omari, J. Maurice Reau, M. Haddad, D. Boudlich, A. Yacoubi, A. Nadiri, Solid State Ionics 132 (2000) 71.
[15] A.-B. Manal, El-D. Fouad, J. Solid State Chem. 184 (2011) 2762.
[16] S.S. Danewalia, K. Singh, S.K. Arya, J. Non-Cryst. Solids 553 (2021), 120471.
[17] L. Galoisy, L. Cormier, G. Calas, V. Briois, J. Non-Cryst. Solids 293 (2001) 105.
[18] M.S. Gaafar, J. Alloys Compd. 475 (2009) 535.
[19] A. Thulasiramudu, S. Buddhudu, J. Quant. Spectrosc. Radiat. Transf. 102 (2006) 212.
[20] G. NagaRaju, M. Srinivasa Reddy, K.S.V. Sudhakar, N. Veeraiah, Opt. Mater. 29 (2007) 1467.
[21] C. Lakshmikanth, B.V. Raghavaiah, N. Veeraiah, J. Lumin. 109 (2004) 190.
[22] M. Subhadra, P. Kistaiah, J. Non-Cryst. Solids 357 (2011) 3442.
[23] R. Balaji Rao, N.O. Gopal, N. Veeraiah, J. Alloys Compd. 368 (2004) 25.
[24] S. Yusub, T. Narendrudu, S. Suresh, D. Krishna Rao, J. Mol. Struct. 1076 (2014) 136.
[25] S. Sindhu, S. Sanghi, S. Rani, A. Agarwal, V.P. Seth, Mater. Chem. Phys. 107 (2008) 236.
[26] M. Farouk, Optik 140 (2017) 186.
[27] T. Raghavendra Rao, Ch.V. Reddy, Ch.R. Krishna, U.S. Udayachandran Thampy, J. Non-Cryst. Solids 357 (2011) 3373.
[28] S. Tanabe, J. Alloys Compd. 408 (2006) 675.
[29] M.S. Gaafar, S.Y. Marzouk, H.A. Zayed, L.I. Soliman, A.H. Serag El-Deen, Curr. Appl. Phys. 13 (2013) 152.
[30] V. Thakur, A. Singh, R. Punia, Ceram. Int. 41 (2015) 10957.
[31] S. Sindhu, S. Sanghi, S. Rani, A. Agarwal, V.P. Seth, Mater. Chem. Phys. 107 (2008) 236.
[32] N. Laorodphan, P. Pooddee, P. Kidkhunthod, P. Kunthadee, W. Tapala, R. Puntharod, J. Non-Cryst. Solids 453 (2016) 118.
[33] A. Ramesh Babu, Ch. Rajyasree, P. Srinivasa Rao, P.M. Vinaya Teja, D. Krishna Rao, J. Non-Cryst. Solids 1005 (2011) 83.
[34] A. Edukondalu, M. Purnima, Ch. Srinivasy, T. Sripathi, A.M. Awasthi, S. Rahman, K. Siva Kumar, J. Non-Cryst. Solids 358 (2012) 2581.
[35] G.P. Singh, P. Kaur, S. Kaur, D.P. Singh, Phys. B 407 (2012) 4269.
[36] A. Yadav, S. Khasa, A. Hooda, M.S. Dahiya, A. Agarwal, P. Chand, Spectrochim. Acta A 157 (2016) 129.
[37] C.R. Kesavulu, R.P.S. Chakradhar, C.K. Jayasankar, J. Lakshmana Rao, J. Mol. Struct. 975 (2010) 93.
[38] H. Wena, P. Tannerb, B. Cheng, J. Mater. Res. Bull. 83 (2016) 400.
[39] G. Srinivasa Rao, P. Narayana Mirthy, R.V.S.S.N Ravikumar, Indian J. Appl. Res. 5 (2015) 2249.
[40] A.M. Abdelghany, A.H. Hammad, J. Spectrochim. Acta A 137 (2015) 39.
[41] J. Tauc, in: J. Tauc (Ed.), Amorphous and Liquid Semiconductors, Plenum, NewYork, 1974, p. 171.
[42] E.A. Davis, N.F. Mott, Philos. Mag. 22 (1970) 903.
[43] S.Y. Marzouk, A.H. Hammad, H.M. Elsaghier, W. Abbas, N.A. Zidan, J. Non-Cryst. Solids 476 (2017) 30.
[44] M.A. Hassan, F. Ahmad, Z.M. Abd El-Fattah, J. Alloys Compd. 750 (2018) 320.
[45] M.A. Hassan, F.M. Ebrahim, M.G. Moustafa, Z.M. Abd El-Fattah, M.M. El-Okr, J. Non-Cryst. Solids 515 (2019) 157.
[46] H.Y. Morshidy, Z.M. Abd El-Fattah, A.A. Abul-Magd, M.A. Hassan, A.R. Mohamed, Opt. Mater. 113 (2021), 110881.
[47] F. Urbach, Phys. Rev. 92 (1953) 1324.
[48] L. Singh, V. Thakur, R. Punia, R.S. Kundu, A. Singh, Solid State Sci. 37 (2014) 64.
[49] E.A. Mohamed, F. Ahmad, K.A. Aly, J. Alloys Compd. 538 (2012) 230.
[50] B. Sumalatha, I. Omkaram, T. Rajavardhana Rao, Ch.L. Raju, J. Mol. Struct. 1006 (2011) 96.
[51] R.P. Sreekanth Chakradhar, K.P. Ramesh, J.L. Rao, J. Ramakrishna, Mater. Res. Bull. 40 (2005) 1028.
[52] V. Sreenivasulu, G. Upender, S.V. VamsiPriya, V. ChandraMouli, M. Prasad, Phys. B 454 (2014) 60.